

Lecture 36

Igneous geochemistry

Reading - White Chapter 7

Today

1. Overview
2. solid-melt distribution coefficients

GG325 L36, F2013

Igneous geochemistry

The chemistry of igneous systems provides clues to a number of important whole-earth processes, including the processes and timing of planetary differentiation, the production and destruction of the lithosphere, and the relationships between magmatic styles, composition and plate-tectonic environment.

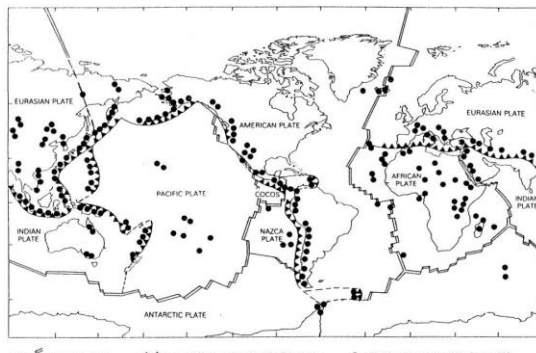


Figure 1.1 Global tectonic map showing the distribution of present-day volcanic activity. Plate boundaries after Condie (1982). Locations of volcanic provinces active within the past 1 Ma after Best (1982). Wilson, "Igneous petrogenesis"

The planet's most volcanically active zones are indicated schematically in the figure.

GG325 L36, F2013

Igneous geochemistry

Magmatism occurs in extrusive (volcanic) and intrusive (plutonic) forms.

Estimates of the **volumes of magmatic rock produced each year** in the four types of plate-tectonic environment are listed in the table below, broken into categories of extrusive (volcanic) and intrusive (plutonic).

Table 1.1 Global rates of Cenozoic magmatism (after McBirney 1984).

Location	Rate (km ³ yr ⁻¹)	
	Volcanic rocks	Plutonic rocks
constructive plate boundaries	3	18
destructive plate boundaries	0.4–0.6	2.5–8.0
continental intra-plate	0.03–0.1	0.1–1.5
oceanic intra-plate	0.3–0.4	1.5–2.0
global total	3.7–4.1	22.1–29.6

Wilson, "Igneous petrogenesis"

- * * Almost entirely basalt
- * * mixture of basaltic, intermediate and silicic

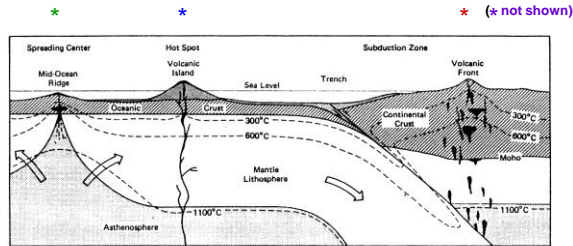


Figure 11.7 Schematic diagram showing divergent and convergent plate boundaries. Tholeiitic basalts erupting at the spreading center create new oceanic crust which is rafted away from the midocean ridge. The lithosphere slab is ultimately incorporated into the mantle in the subduction zone. Calc-alkaline magmas are produced in this environment. Isotherms (dashed lines) are defined upward by ascending magmas in both locations, and downward in the subduction zone itself; these control the *P-T* regime of metamorphism. Hot-spot igneous activity is illustrated by intraplate volcanism located spatially between these two tectonic environments.

GG325 L36, F2013

Igneous geochemistry

We've already seen that the Earth's crustal rocks are bimodal in density, and by inference, composition.

Here's a composition histogram.

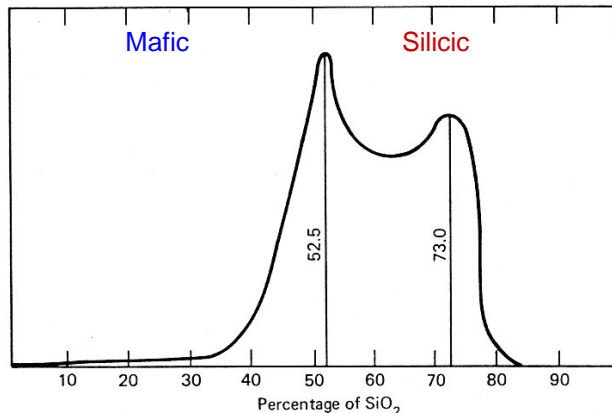
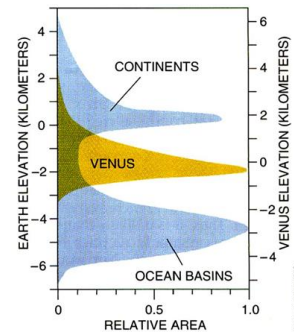


Figure 5.1 The frequency distribution of silica percentage in analyses of igneous rocks.



SURFACE ELEVATIONS are distributed quite differently on the earth (blue) and on Venus (gold). Most places on the earth stand near one of two prevailing levels. In contrast, a single height characterizes most of the surface of Venus. (Elevation on Venus is given with respect to the planet's mean radius.)

Taylor and McLennan, *Sci. Amer.* 1996

GG325 L36, F2013

Igneous geochemistry

The magmas that ultimately produce the crust are commonly referred to as **mafic** (rich in Mg and Fe, poor in Si) and **silicic** (the opposite).

But, the bimodality is far from perfect.

A **range of compositions and processes** form more of a **continuum** of igneous rock compositions.

Some magmas represent **melts of the mantle** whereas others represent **melts of the crust**, particularly on the continents.

Other magmas are **mixtures** thereof.

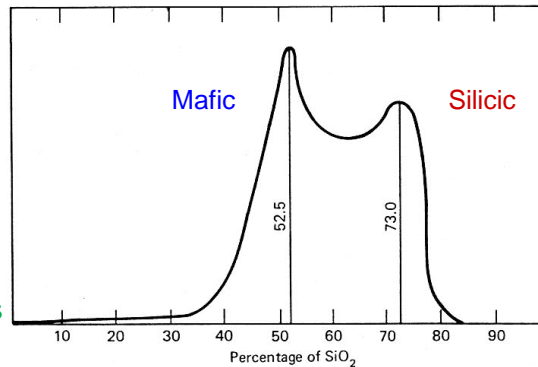


Figure 5.1 The frequency distribution of silica percentage in analyses of igneous rocks.

GG325 L36, F2013

Early Igneous geochemistry History

By the early 1900s, a great deal was already known about the chemical compositions of igneous rocks.

However, an understanding of why certain compositions occurred in certain places had to wait until the **advent of plate tectonics theory** in the 1960s.

The first large compendium of major-element analyses of igneous rocks from around the world was published in 1917.

Using 5159 samples, it demonstrated that most igneous rocks are mixtures of just **10 major elements** (O, Si, Al, Mg, Fe, Ca, Ti, Na, K, P), plus minor (usually <1%) amounts of Mn and H₂O.

GG325 L36, F2013

Major Elements

Chemical compositions of igneous rocks are usually reported as **weight % (wt%)** of each element as an **oxide**.

There are typically 9 major and 2 minor element oxides listed in a rock analysis.

This is true when Fe is reported as total FeO or total Fe_2O_3 .

Sometimes both oxidation states [Fe^{2+} (FeO) and Fe^{3+} (Fe_2O_3)] are analyzed and reported separately, as in the olivine thermometry homework problem we had earlier this semester.


Be sure to check this aspect when scrutinizing rock analysis data.

GG325 L36, F2013

Igneous geochemistry

The early data base was strongly biased toward rocks from easily-accessed locations, nearly all on land, so some details about global variations in composition have changed.

 SiO_2 content in igneous rocks is **bimodal** , as is **CaO** and **K_2O**

 Each of the other major element oxides has **one** dominant range of composition

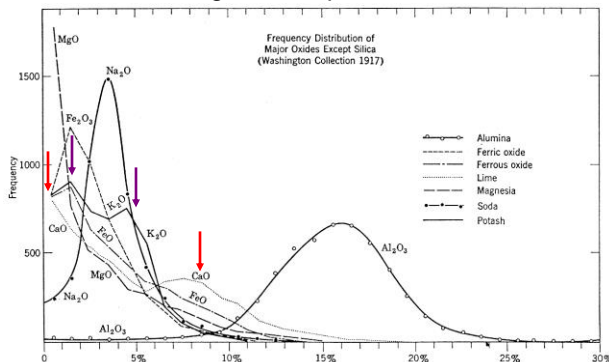


Figure 5.2 The frequency distribution of the percentages of the major oxides in analyses of igneous rocks. (Richardson and Sneesby, *Mineralog. Mag.* 19, 309, 1922)

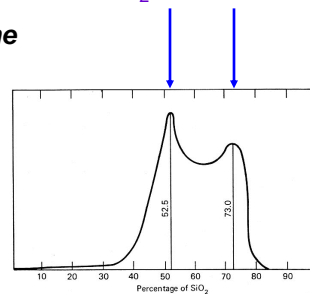


Figure 5.1 The frequency distribution of silica percentage in analyses of igneous rocks.

GG325 L36, F2013

Igneous geochemistry

The major elements are found in different proportions in the main minerals of igneous rocks, and these minerals vary in proportion and composition with rock type.

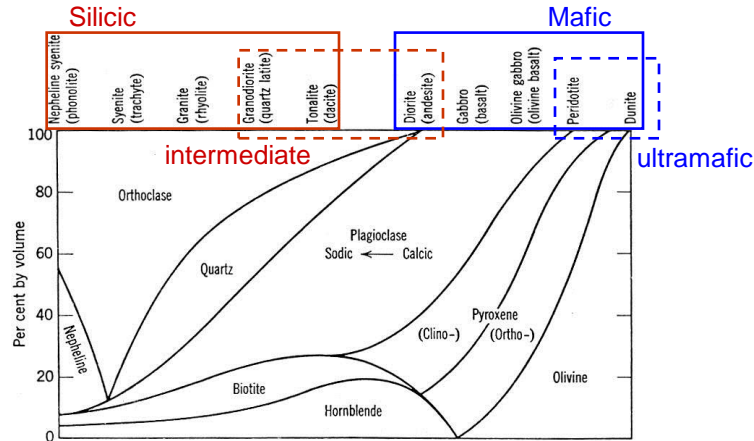


Figure 5.3 Approximate mineralogical composition of the commoner types of igneous rocks (effusive types in brackets).

GG325 L36, F2013

Igneous geochemistry

Some of you have already taken igneous petrology (the study of the distributions of minerals in igneous rocks and their relationship to the conditions of melting and crystallization).

Many others of you will be taking such a course, so we won't focus here on the major element or mineral compositions of igneous rocks.

These figures summarize one of the common *chemical* classifications of the main volcanic and plutonic rock types in terms of SiO_2 and total alkalis (TAS = $\text{Na}_2\text{O} + \text{K}_2\text{O}$) concentrations in wt%.

TAS diagrams

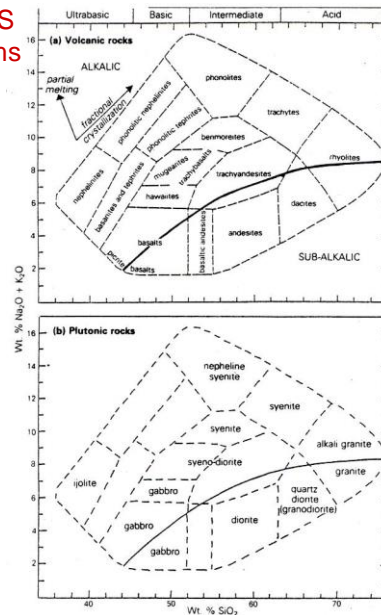


Figure 1.2 Nomenclature of normal (i.e. non-potassic) igneous rocks (Iai) after Cox et al. 1979). The dividing line between alkalic and sub-alkalic magmas series is from Miyashiro (1978).

GG325 L36, F2013

Mafic

TABLE 8-1 Chemical Compositions of Some Common Igneous Rocks

	1	2	3	4	5
	Oceanic alkali olivine basalt	Oceanic tholeiite basalt	Continental tholeiite basalt	Island arc dunite	Island arc andesite
SiO ₂	50.48	49.20	52.05	39.53	58.60
TiO ₂	2.25	2.63	1.70	0.01	0.89
Al ₂ O ₃	18.31	16.99	12.43	0.93	15.38
Fe ₂ O ₃	3.21	2.72	5.18	0.65	2.22
FeO	6.03	7.77	10.08	7.62	6.71
MnO	0.21	0.18	0.24	0.12	0.18
MgO	4.21	6.44	3.95	48.83	3.22
CaO	7.21	10.46	7.33	Trace	7.02
Na ₂ O	4.80	3.01	2.76	Trace	3.84
K ₂ O	1.93	0.14	2.07	—	1.46
P ₂ O ₅	0.74	0.23	0.28	—	0.25
H ₂ O ⁺	0.46	0.70	1.80	0.89	0.30
H ₂ O ⁻	0.38	0.95	0.36	0.16	0.07
Other			1.41		
Total:	100.22	99.92	100.33	100.15	100.14
K/Rb	267	950	498	215	807
Rb/Sr	0.09	0.02	0.04	0.025	0.038
⁸⁷ Sr/ ⁸⁶ Sr	0.7033	0.7034	0.7064	0.7091	0.7036

Sources:

1. Cenozoic alkali olivine basalt, Guadalupe Island, data from A. E. J. Engel et al., 1965, *Bull. Geol. Soc. Am.*, v. 76, p. 725, and Z. E. Pezerman and C. E. Hedge, 1971, *Bull. Geol. Soc. Am.*, v. 82, p. 495.
2. Cenozoic tholeiite basalt, Atlantic Ocean, depth 2,910 m, 20° 40' S, 13° 16' W; data from A. E. J. Engel and C. G. Engel, 1964, *Science*, v. 144, p. 1332, and P. W. Gast, 1967, *Basalts (Poldervaart Treatise)*, Wiley (Interscience Division), v. 1, p. 325.
3. Jurassic tholeiite basalt, Niamezi region, Karoo Basin, South Africa; data from K. G. Cox et al., 1965, *Phil. Trans. Roy. Soc. Lond., ser. A*, v. 257, p. 71, and W. I. Manson, 1968, *J. Petrol.*, v. 9, p. 30.
4. Permian dunite, Dun Mt., New Zealand; data from J. J. Reed, 1959, *New Zealand J. Geol. Geophys.*, v. 2, p. 16, and A. M. Stueber and V. R. Murthy, 1966, *Grochim. Cosmochim. Acta*, v. 30, pp. 1247–1248.
5. Quaternary pyroxene andesite, Talasea, New Britain; data from G. G. Lowder and I. S. E. Carmichael, 1970, *Bull. Geol. Soc. Am.*, v. 81, p. 27, and Z. E. Peterman et al., 1970, *Bull. Geol. Soc. Am.*, v. 81, p. 314.

Silicic

	6	7	8	9	10
	Island arc rhyolite	Continental rift leucite nephelinite	Gabbro of continental layered mafic pluton	Continental anorthosite	Continental batholith quartz monzonite
SiO ₂	74.22	39.77	48.08	53.40	65.49
TiO ₂	0.28	3.82	1.17	0.77	0.65
Al ₂ O ₃	13.27	12.53	17.22	23.96	14.49
Fe ₂ O ₃	0.88	6.02	1.32	0.91	2.11
FeO	0.92	8.62	8.44	3.02	2.90
MnO	0.05	0.27	0.16	—	0.10
MgO	0.28	4.45	8.62	1.88	2.45
CaO	1.59	11.88	11.38	9.85	4.29
Na ₂ O	4.24	4.86	2.37	4.17	2.80
K ₂ O	3.18	5.35	0.25	0.80	3.66
P ₂ O ₅	0.05	1.35	0.10	0.18	0.21
H ₂ O ⁺	0.80	0.60	1.01	0.56	0.56
H ₂ O ⁻	0.23	0.32	0.05	0.69	0.05
Other				0.43	0.15
Total:	99.99	99.84	100.17	100.06	99.91
K/Rb	251	352	550	>1,000	232
Rb/Sr	1.0	0.058	0.022	<0.01	0.311
⁸⁷ Sr/ ⁸⁶ Sr	0.7054	0.7051	0.7076	0.7053	0.7086

Sources:

6. Average Quaternary rhyolite, Taupo volcanic zone, New Zealand; data from A. Ewart and J. J. Stupp, 1968, *Grochim. Cosmochim. Acta*, v. 32, pp. 704, 712.
7. Quaternary leucite nephelinite, War Cemetery Flow, Nyiragongo volcano, Congo; data from K. Bell and J. L. Powell, 1969, *J. Petrol.*, v. 10, pp. 546, 549.
8. Chilled border gabbro, Tertiary Skaergaard intrusion, Greenland; data from L. R. Wager and G. M. Brown, 1967, *Lavred Igneous Rocks*, Freeman, p. 158, pp. 193–194.
9. Gabbroic anorthosite, Precambrian Adirondack massif, New York; data from A. F. Buddington, 1939, *Geol. Soc. Am. Memoir* 7, p. 30, and S. A. Heath and H. W. Fairbairn, 1969, *N. Y. State Museum* 18, p. 99.
10. Cretaceous Butte Quartz Monzonite, Kain quarry, Boulder batholith, Mont.; data from A. Knopf, 1957, *Am. J. Sci.*, v. 255, p. 89, and B. R. Doe et al., 1968, *Econ. Geol.*, v. 63, p. 898.

GG325 L36, F2013

Igneous geochemistry

One potential compositional evolution path of basaltic magmas as a function of Temperature, SiO₂, and MgO is:

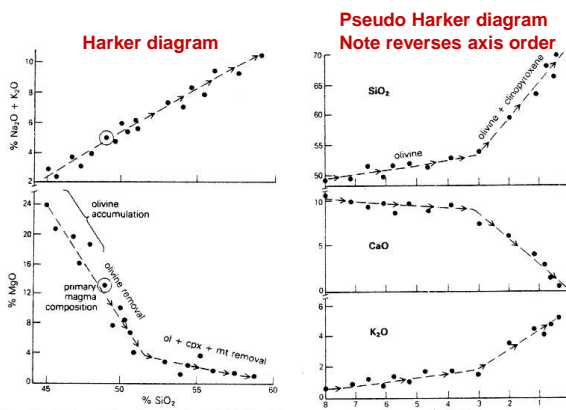


Figure 2.1 Harker variation diagrams of wt. % Na₂O + K₂O and wt. % MgO versus wt. % SiO₂ for a suite of cogenetic volcanic rocks related by fractional crystallization of olivine, clinopyroxene and magnetite. The highly magnesian basalts (MgO >12%) may have accumulated olivine by crystal settling. This should be evident in their petrography, i.e. the samples should be highly olivine phyric.

Figure 2.2 Harker-type variation diagrams, with wt. % MgO as abscissa, for a cogenetic suite of volcanic rocks related by fractional crystallization of olivine and clinopyroxene.

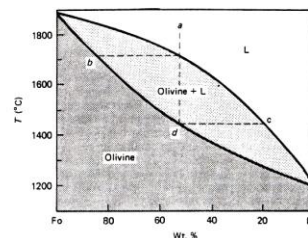


Figure 11.14 Phase diagram for the system forsterite (Mg₂SiO₄)-fayalite (FeSiO₂), illustrating how fractional crystallization affects a solid solution series. Olivine crystals forming from a melt with initial composition a will range in composition from b to some point past d.

inflections in the trends indicate the appearance or disappearance of minerals.

GG325 L36, F2013

Igneous geochemistry

We will instead focus mainly on evidence provided by the **trace elements**, which are covered in less detail in petrology courses.

Unlike major element analyses, trace element data are usually reported as an element's relative concentration by mass (e.g., ppm, ppb).

By definition, ***trace elements are present at concentrations less than about 0.1 wt%.***

GG325 L36, F2013





Igneous geochemistry

As we saw last week, trace elements provide key insights into the composition of the mantle.

We will look in the next few days at how they are used as tracers of the composition of mantle and crustal **source rocks** that melt to produce magmas.

Trace elements also yield important information about the processes and conditions of **melting** and **crystallization**.

Trace elements usually do not form the major rock-forming phases. Instead, they **partition** themselves among the different major phases as “contaminants”, according to

-  ionic radius
-  ionic charge
-  electronegativity
-  lattice energy of substitution site

GG325 L36, F2013

"Goldschmidt's Rules"

These outline the conditions for trace element partitioning between igneous phases.

Ions will substitute readily for each other in a mineral lattice if...

1. **Size:** Their ionic radii differ by <15%.
2. **Charge:** They have the same charge or ± 1 unit of charge difference (*substitution with greater charge differences may occur but to a significantly lesser degree*).

Of two ions with the charge and radius to occupy a lattice site...

3. The ion with the higher **ionic potential** (z/r) is favored because it will make stronger bonds.

A fourth rule was added more recently by Ringwood:

4. The ion with the most similar **electronegativity** to that of the major element being replaced will be favored because it destabilizes the crystal lattice the least.

GG325 L36, F2013

Trace element partitioning example

This diagram shows contours of the clinopyroxene-melt distribution (partition) coefficient for various ions as a function of charge and radius (i.e., primarily rules #1 and #2).

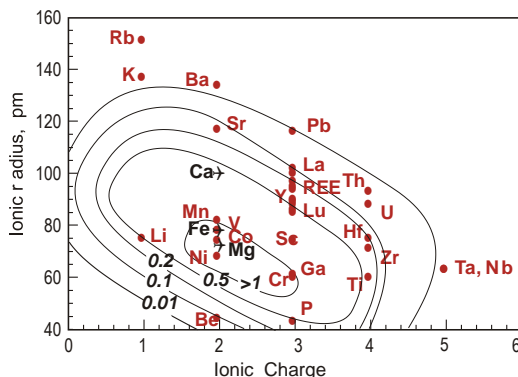


Figure 7.10. Ionic radius (picometers) vs. ionic charge contoured for clinopyroxene/liquid partition coefficients. Cations normally present in clinopyroxene are Ca^{2+} , Mg^{2+} , and Fe^{2+} , shown by \rightarrow symbols. Elements whose charge and ionic radius most closely match that of the major elements have the highest partition coefficients.

modified from White, Geochemistry

GG325 L36, F2013

Trace element partitioning

Size is fairly intuitive control, since the substituting ion needs to fit into a mineral lattice: Too big or too small a won't be energetically stable.

Charge is also intuitive, since charge must be balance within a lattice and if a charge imbalance is generated by a substitution, a second substitution must occur to correct for this.

Electronegativity is harder to visualize, but the disruption of replacing a greedy element with a giving element or vice versa is too much for a lattice to take.

example: we rarely see substitutions of like-charge and like-size pairs like Na^+ - Cu^+ and Ca^{+2} and Cd^{+2} due to electronegativity differences.

GG325 L36, F2013

Trace element distribution

We can determine whether a particular substitution is favored or not by using the solid-melt distribution (partition) coefficient.

Recall the equation for the simple case of melt + one solid:

$${}^A k_d = [\text{conc. of A}]_{\text{solid}} / [\text{conc. of A}]_{\text{melt}}$$

For a multi-phase system (one melt + more than one solid; e.g., several minerals), we use the **bulk distribution coefficient**:

$$\text{Bulk } {}^A k_d = {}^A K_d = D_A = \bar{k}_A = [\text{modal conc. of A}]_{\text{solids}} / [\text{conc. of A}]_{\text{melt}}$$

GG325 L36, F2013

Trace element distribution

K_d and D_A values tell us about the tendency of an element to be proportioned between coexisting melt and solids.

$D_A > 1$ The element is **compatible** (a.k.a. “captured”).

$D_A = 1$ The element is **neutral** (a.k.a. “camouflaged”).

$D_A < 1$ The element is **incompatible** (a.k.a. “released”).

GG325 L36, F2013

Trace element distribution

A **rigorous definition** of bulk k_d (“D”) for a multiphase solid (a, b, c, ..., j) + one melt system is:

$$D = \alpha k_d^a + \beta k_d^b + \gamma k_d^c + \dots \chi k_d^j = \sum X_j k_d^j$$

where α , β , γ , and χ are the proportions of the minerals that comprise the solid,

and k_d^a , k_d^b , k_d^c , ..., k_d^j are the mineral-melt partition coefficients for each of the different minerals, a, b, c, ..., j that are in equilibrium with the melt.

X_j is the mole fraction of mineral a to j present.

GG325 L36, F2013

Trace element distribution

in addition to ionic charge, radius, and electronegativity, the **temperature** and **pressure** of the system play a key role in trace element substitution, because as we've seen throughout the course, T and P determine *which* solids will be present in a given system.

Also, *structural controls* on crystal lattice energy are such that each type of lattice site has a specific *energy of ion substitution*.

For a given crystal lattice, that energy is a function of T and P.

GG325 L36, F2013

Trace element distribution

To summarize, the energy of substitution is minimized (made most favorable) for substitution by the "right" ion;

that is, the one with the best combination of

- ✓ **size,**
- ✓ **charge,**
- ✓ **electronegativity.**
- ✓ **as a function of T and P**

A substitution into a phase becomes less favorable (i.e., k_d goes down) the more any of these values vary from the ideal.

The incompatible elements have $k_d < 1$ in all the common mantle minerals (and $D < 1$ in mantle rocks) because their substitution energies are high in all of these minerals.

GG325 L36, F2013

Trace element distribution

We can understand quite a lot about k_d differences by observing how k_d varies in a given mineral as a function of ionic size in an *iso-charged series* (same valence or oxidation number).

This helps us understand the structural controls on the distribution of ions between a mineral and a melt.

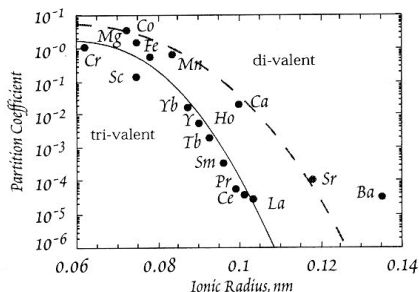


Figure 7.11. Partition coefficients for di- (dashed) and tri-valent ions between olivine and silicate liquid as a function of ionic radius. Points are experimentally determined partition coefficients, lines are partition coefficients predicted from equations 7.17 and 7.20 using $r_0 = 58$ pm, $\sigma = 0.25$ MPa, $K = 95.3$ Mpa, and $\Delta C_0 = 551$ /mol-K
modified from White, *Geochemistry*

Here's an example for olivine and melt.

These types of diagrams are known as **Onuma diagrams**, after their originator.

Examples for plagioclase and clinopyroxene are given in the next three slides.

GG325 L36, F2013

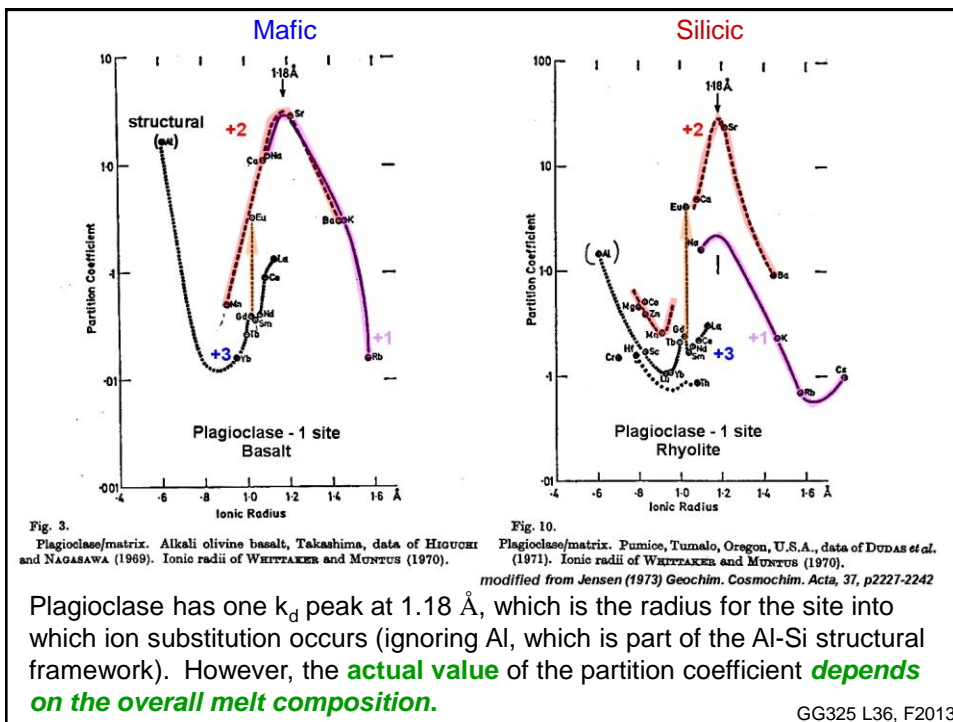


Fig. 3. Plagioclase/matrix. Alkali olivine basalt, Takashima, data of HIGUCHI and NAGASAWA (1969). Ionic radii of WHITTAKER and MUNTUS (1970).

Fig. 10. Plagioclase/matrix. Pumice, Tumalo, Oregon, U.S.A., data of DUDAS *et al.* (1971). Ionic radii of WHITTAKER and MUNTUS (1970).
modified from Jensen (1973) *Geochim. Cosmochim. Acta*, 37, p2227-2242

Plagioclase has one k_d peak at 1.18 \AA , which is the radius for the site into which ion substitution occurs (ignoring Al, which is part of the Al-Si structural framework). However, the **actual value** of the partition coefficient **depends on the overall melt composition**.

GG325 L36, F2013

Trace element distribution

Lava composition and temperature determine the An number of the plagioclase feldspar.

Remember...

★An₁₀₀ = 100% anorthite
(CaAl₂Si₂O₈)

★An₀ = 100% albite
(NaAlSi₃O₈)

★An₅₀ = an equal mixture
of the two

Notice that K_d^{Sr} varies from 5 in
basalt to 50 in rhyolite.

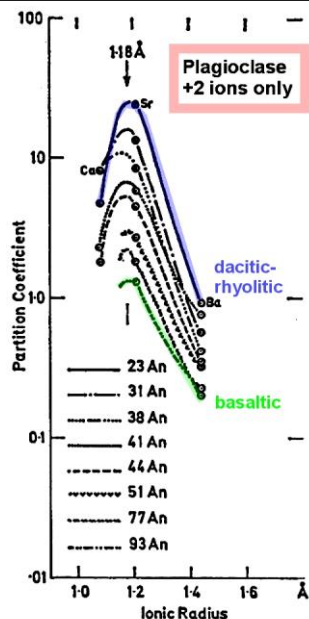


Fig. 12. Plagioclase/matrix plots of the divalent peak for 8 samples showing relationship between height of the peak and An content of the plagioclase. Data largely from DODAS *et al.* (1971), EWART and TAYLOR (1969) and PHILPOTS and SCHNETZLER (1970).
from Jensen (1973)

GG325 L36, F2013

Trace element distribution

The double peak in the augite curve is from substitution into two structural sites with radii of 0.79 Å and 1.01 Å.

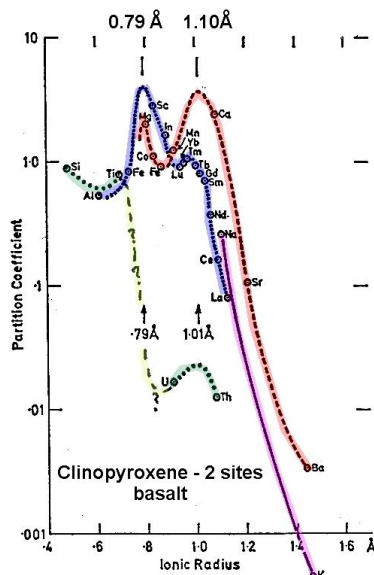


Fig. 1. Partition coefficient vs ionic radius for augite/matrix. Olivine alkali basalt, Takashima, data of ONUMA *et al.* (1968). Ionic radii of WHITTAKER and MUNTUS (1970).

from Jensen (1973) *Geochim. Cosmochim. Acta*, 37, p2227-2242

GG325 L36, F2013

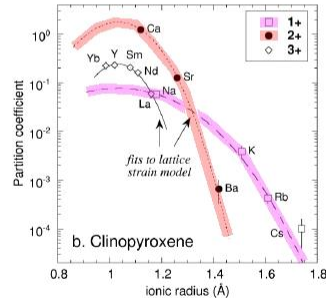
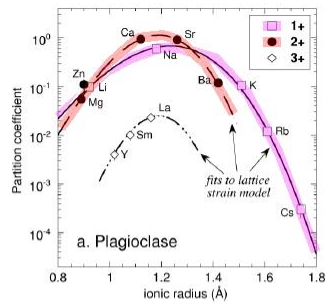


Figure 4. Fits of lattice strain model to experimental mineral-melt partition coefficients for (a) plagioclase (run 90-6 of Blundy and Wood 1994) and (b) clinopyroxene (run DC23 of Blundy and Dalton 2000). Different valence cations, entering the large cation site of each mineral, are denoted by different symbols. The curves are non-linear least squares fits of Equation (1) to the data for each valence. Error bars, when larger than symbol, are 1 s.d. Ionic radii in VIII-fold coordination are taken from Shannon (1976). *Blundy and Wood, IMA, 2003*

GG325 L36, F2013

Trace element distribution

The very latest models for partition coefficients incorporate *lattice strain* and *electrostatic factors* to derive best-fit parameterizations. Notice that the plagioclase peak is still at 1.18 Å.

Also note that only the peak at 1.10 Å is shown in this clinopyroxene diagram (i.e., the 0.79 Å peak is still there, but the figure's scale stops at 0.8 Å).

If you need a k_d value for a given element but can't find a published value, you can estimate it from such model curves.

Trace element distribution

Compilations of measured values for mineral-melt distribution coefficients for many of the geochemically important elements are given in the next two slides (as well as in your reading).

There are two tables: one for **mafic lavas** and one for **silicic lavas**.

As we saw in the Onuma diagrams for plagioclase, the k_d values for a given mineral are often quite *different* in **mafic** vs. **silicic** melts.

These two tables are relatively complete, but the data are only for magmas at atmospheric pressure and the data are quite old.

Slightly different values apply at higher pressures, but we'll assume for the purposes of this course that we can use low- and moderately high-pressure values interchangeably.

*Note: when melt solidifies rapidly, it forms a **glassy "matrix"** of an igneous rock. Slow cooling magmas tend to have little to none of this.*

GG325 L36, F2013

Trace element distribution coefficients

Mafic

TABLE 5.2a. Mineral/matrix partition coefficients of elements in basaltic and andesitic rocks

Henderson, *Inorganic Chemistry*, 1984

	Olivine		Orthopyroxene		Clinopyroxene		Amphibole		Plagioclase		Phlogopite (one determination)	Garnet	
	Range	Average	Range	Average	Range	Average	Range	Average	Range	Average		Range	Average
3 Li						0.26	*	0.12, 0.19	*	0.20	*		
11 Na	0.012-0.024	0.02	0.075	*		0.27	*	0.72, 0.80	*				
12 Mg	4.5-8.0	6.1	4, 7	*		2-5	*	2.8, 4.8	*				
13 Al	0.012	*	0.3	*		0.21-0.6	0.3			1.6-2.1			
19 K	0.002-0.008	0.007	0.01, 0.02	*		0.002-0.27	0.03	0.33-0.86	0.60	0.02-0.36	0.17	2.7	
20 Ca	0.01-0.04	0.03	0.2, 0.4	*				1.1, 3.0	*				
21 Sc	0.14-0.22	0.17	1.2	*		1.7-3.2	2.7	2.2, 4.2	*			2.6-5.4	4
22 Ti						0.8	*						
23 V	0.03	*	0.6	*		0.8-1.9	1.3						
24 Cr	1.1-3.1	2.1	10	*		4.7-20	8.4	0.10, 1.6	*			0.06, 0.29	*
25 Mn	0.8-1.8	1.2	1.4	*		0.6-1.3	0.9			0.05	*		
26 Fe ⁺⁺	1.2-3.0	1.9	1.8	*		0.6-1.0	0.8						
26 Fe ³⁺			0.75	*		0.37-0.86	0.53						
27 Co	2.8-5.2	3.8	2, 4	*		0.7-2.8	1.2	1.4, 1.8	*			0.7-1.8	1.1
28 Ni	8-19	14	5	*		1.4-4.4	2.6						
30 Zn	0.7	*				0.41	*	0.42, 0.69	*				
31 Ga	0.04	*	0.7	*		0.39-0.58	0.40			0.85-1.3	1.0		
37 Rb	0.0002-0.011	0.006	0.02, 0.03	*		0.001-0.28	0.04	0.04-0.4	0.25	0.03-0.50	0.10	3.1	
38 Sr	0.0001-0.02	0.01	0.01, 0.02	*		0.07-0.43	0.14	0.19-1.02	0.57	1.3-2.9*	1.8	0.08	
49 In	0.06	*	0.45	*		1.7	*	2.2, 3.1	*				
55 Cs	0.0004	*				0.002-0.018	0.01	0.05, 0.20	*	0.025	*		
56 Ba	0.0001-0.011	0.006	0.012, 0.014	*		0.002-0.39	0.07	0.10-0.44	0.31	0.05-0.59	0.23	1.1	
57 La						0.08	*	0.17-0.44	0.27	0.14	*	0.03, 0.08	*
58 Ce	0.009	*	0.003-0.04	0.02		0.17-0.65	0.34	0.09-0.54	0.34	0.06-0.30	0.14	0.03	0.05
60 Nd	0.007, 0.010	*	0.03, 0.06	*		0.32-1.3	0.6	0.19	*	0.02-0.20	0.08	0.03	
62 Sm	0.003-0.015	0.009	0.01-0.10	0.05		0.43-1.8	0.9	0.34-1.46	0.91	0.02-0.20	0.08	0.03	0.07-1.25
63 Eu	0.006, 0.010	*	0.02, 0.08	*		0.48-2.0	0.9	0.36-1.49	1.01	0.06-0.73	0.32	0.03	0.3-1.5
64 Gd	0.012	*				0.82, 0.88	*	0.51-1.7	1.1	0.03-0.21	0.10	*	2.1, 5.2
65 Tb			0.05	*		1.0	*	1.02-2.0	1.4	0.03	*	*	4.1, 7.1
66 Dy	0.009, 0.014	*	0.12, 0.29	*		0.56-1.46	1.1	0.64	*	0.01-0.20	0.09	0.03	13, 24
67 Ho													*
68 Er	0.009, 0.017	*	0.16, 0.46	*		0.53-1.3	1.0	0.48	*	0.02-0.24	0.08		
69 Tm						1.1	*					0.03	
70 Yb			0.11-0.67	0.34		0.48-1.3	1.0	0.46-1.42	0.97	0.006-0.30	0.07		4-53
71 Lu			0.11	*		0.67, 1.0	*	0.44-1.31	0.89	0.03-0.24	0.08	0.04	5-57
72 Hf													0.3, 0.6
82 Pb										0.10-0.67	0.26		
90 Th						0.003-0.05	0.02						
92 U	0.0024, 0.0027	*				0.004-0.08	0.04			0.009	*		

* Where only one or two determinations are available, an average is not given; the values are quoted in the range column.

GG325 L36, F2013

Trace element distribution coefficients

Silicic

TABLE 5.2b. Mineral/matrix partition coefficients of elements in dacitic and rhyolitic rocks

Henderson, *Inorganic Chemistry*, 1984

	Orthopyroxene		Clinopyroxene		Amphibole		Plagioclase		Alkali Feldspar		Biotite (1 or 2 determinations)	Garnet		Magnetite	
	Range	Average	Range	Average	Range	Average	Range	Average	Range	Average		Range	Average	Range	Average
3 Li	0.16, 0.21	*					0.27-0.66				0.39				
11 Na	0.03-0.1	0.06	0.09-0.14	0.11	0.08	*	1.2-3.1	1.5			0.10				
12 Mg	50-160	100					0.03-0.5	0.3	0.05-0.33	0.21	22				
19 K	0.0006, 0.002	*					0.08-0.33	0.19	0.64-2.2	1.4	2.6, 5.6	0.02	*		
20 Ca	0.55-2.3	1.4	8-12	10	1.8	*	1.8-4.9	3.4	0.10-3.8	1.9	0.62			0.3-0.5	0.4
21 Sc	6.0-7.7	6.9	18-28	22	20	*	0.01-0.20	0.07			11.3	10.2-20.2	16.0	3.3-4.5	3.9
23 V	4.4-10	6													
24 Cr	0.6-3	1.6	90	*			0.03-0.7	0.2			19			5-20	11
25 Mn	29, 34	*					0.03-0.31	0.18	0.03-0.52	0.18	6.0				
27 Co	2.1-3.6	2.9	6.0-11	8	45	*	0.04-0.5	0.15			29	1.7-3.6	2.6	19-35	28
30 Zn	0.8-1.0	0.9			7	*	0.26-0.60	0.38			20			10-14	12
37 Rb	0.0005-0.29	0.09	0.09	*			0.02-0.46	0.09	0.11-0.80	0.38	3.3, 3.5	0.009	*		
38 Sr	0.009, 0.05	*					1.5-8.8	6†	3.6-26	9.4	0.12, 0.36	0.02	*		
39 Y	0.9	*													
49 In											3.9				
55 Cs	0.3	*					0.01-0.13	0.05			2.4				
56 Ba	0.003-0.03	0.02	0.02, 0.06	*	0.035	*	0.30-0.92	0.50	2.7-12.9	6.6	6.4, 8.7	0.017	*	0.05-0.08	0.07
57 La	0.50-0.90	0.65	0.5-0.8	0.6	0.85	*	0.24-0.49	0.32			0.32	0.28-0.54	0.39	0.24-0.88	0.53
58 Ce	0.08-1.03	0.46	0.6-1.2	0.9	0.43-1.8	1.2	0.11-0.40	0.24	0.04	*	0.04, 0.38	0.35-0.93	0.62	0.28-1.15	0.61
60 Nd	0.11-1.20	0.62	1.4-2.9	2.1	1.0-4.3	3.2	0.06-0.29	0.19	0.03	*	0.04	0.53-0.73	0.63	0.35-1.80	0.88
62 Sm	0.13-1.6	0.7	2.1-3.3	2.7	1.6-8.2	5.4	0.05-0.22	0.13	0.02	*	0.06, 0.39	0.76-5.5	2.2	0.39-1.85	0.93
63 Eu	0.11-1.0	0.5	1.6-2.3	1.9	1.2-5.9	3.6	0.82-4.2	2.0	1.13	*	0.15, 0.33	0.17-1.37	0.7	0.28-0.96	0.58
64 Gd	0.17-2.2	1.1	2.0-4.8	3.1			0.11-0.24	0.16			0.08, 0.44	5.3-13.6	7.7		
65 Tb	0.8-1.6	1.2	2.0-4.1	3.0	3.0	*	0.10-0.22	0.15			0.39	7.2-19.6	1.2	0.36-1.50	0.84
66 Dy	0.26-1.3	0.7	2.2-4.0	3.3	2.3-14	9	0.04-0.45	0.13	0.006	*	0.10	29	*	0.3-1.4	0.8
67 Ho												18.4-35	28		
68 Er	0.43-0.73	0.61			2.4-11	8	0.03-0.08	0.05	0.006	*	0.16	43	*		
69 Tm	0.8-1.9	1.4			5	*	0.1-0.2	0.1						0.5-1.2	0.8
70 Yb	0.73-1.2	1.0	1.6-2.8	2.1	1.9-9	6.2	0.02-0.30	0.08	0.012	*	0.18, 0.67	26-67	43	0.2-0.6	0.4
71 Lu	0.76-1.4	1.1	2.0-2.6	2.3	1.8-6	4.5	0.03-0.11	0.06			0.74	24-64	38	0.2-0.6	0.4
72 Hf	0.04, 0.2	*	0.20-0.55	0.34	6	*	0.02-0.17	0.07			2.10			0.2-0.6	0.3
73 Ta	0.2-0.7	0.5	0.1-0.8	0.4	0.3	*	0.02-0.09	0.05						0.8-1.8	1.3
82 Pb							0.29-0.78	0.45	0.84-1.4	1.0					
90 Th	0.13-0.12	0.15	0.01-0.25	0.13	0.22	*	0.01-0.09	0.04			0.31			0.04-0.20	0.11
92 U	0.09	*	0.03	*	0.40	*	0.01-0.07	0.03						0.14	*

GG325 L36, F2013

Trace element distribution

As mentioned above, the “bulk K_d ”, D , is a weighted average of all the individual mineral-melt K_d s for the system.

Let's calculate bulk K_d values for Rb and Co for melting within the shallow mantle of a basalt composed of 45% olivine, 35% opx and 20% cpx using the data from the Henderson tables as an example.

We will use

$$K_d = \alpha K_d^a + \beta K_d^b + \gamma K_d^c$$

	K_d^{ol}	K_d^{opx}	K_d^{cpx}	Bulk K_d or D
Rb	0.006	~0.03	0.14	$0.45*0.006 + 0.35*0.03 + 0.2*0.04 =$ 0.021
Co	3.8	~3	1.2	$0.45*3.8 + 0.35*3 + 0.2*1.2 =$ 3.0

Rb behaves **incompatibly**, **Co** behaves **compatibly** in this system.